Quasiparticle self-consistent *GW* calculations for PbS, PbSe, and PbTe: Band structure and pressure coefficients

A. Svane,[1] N. E. Christensen,[1] M. Cardona,[2] A. N. Chantis,[3] M. van Schilfgaarde,[4] and T. Kotani[5]
[1]*Department of Physics and Astronomy, Aarhus University, DK-8000 Aarhus C, Denmark*
[2]*Max-Planck-Institut für Festkörperforschung, Heisenbergstraße 1, D-70569 Stuttgart, Germany*
[3]*Theoretical Division, Los Alamos National Laboratory, Los Alamos, New Mexico 87545, USA*
[4]*School of Materials, Arizona State University, Tempe, Arizona 85287-6006, USA*
[5]*Department of Applied Physics and Mathematics, Tottori University, Tottori 680-8552, Japan*
(Received 29 March 2010; published 18 June 2010)

The electronic band structures of PbS, PbSe, and PbTe in the rocksalt structure are calculated with the quasiparticle self-consistent *GW* (QS*GW*) approach with spin-orbit coupling included. The semiconducting gaps and their deformation potentials as well as the effective masses are obtained. The *GW* approximation provides a correct description of the electronic structure around the gap, in contrast to the local-density approximation, which leads to inverted gaps in the lead chalcogenides. The QS*GW* calculations are in good quantitative agreement with experimental values of the gaps and masses. At moderate hole doping a complex filamental Fermi-surface structure develops with ensuing large density of states. The pressure-induced gap closure leads to linear (Dirac-type) band dispersions around the L point.

DOI: 10.1103/PhysRevB.81.245120 PACS number(s): 71.20.Nr, 71.15.Qe, 72.80.Jc, 71.10.−w

I. INTRODUCTION

The lead chalcogenides PbX (with X=S. Se, or Te) are of great importance for infrared detection and lasing devices,[1–3] and furthermore find applications as thermoelectric materials,[4–6] as window coatings[7] and in solar-energy panels.[8] With Tl doping PbTe may even exhibit superconductivity.[9,10] The lead chalcogenides crystallize in the rocksalt structure at normal pressure. Their electronic structures[11,12] are characterized by small direct semiconducting gaps, which occur at the L point of the Brillouin zone (BZ). The gaps measured at low temperature are 0.286 eV, 0.165 eV, and 0.19 eV for PbS, PbSe, and PbTe, respectively.[13] In contrast to most other semiconductors, the gaps of the lead chalcogenides increase with temperature and decrease under pressure.[14–18] The pressure effect has been explained[19] as originating from the relatively deep lying Pb *s* state together with level repulsion around the L point. These authors also explained other trends in the series including alloys and band offsets in heterostructures. The trends in optical properties[20] were analyzed by theory based on the local-density approximation (LDA), and recently the elastic properties, including phonon spectra and thermodynamic properties[21,22] were studied based on LDA calculations. The LDA band structures (with all relativistic effects included) reproduce well the valence bands of the PbX compounds measured in photoemission,[23,24] and also a narrow semiconducting gap is found,[20,22] in spite of the failure of the LDA when calculating the gap of most other semiconductors. Closer inspection reveals that the LDA, in fact, leads to the valence-band maximum (VBM) and conduction-band minimum (CBM) states being interchanged.[19,25] These states have the same L_6 symmetry but different parity and orbital character and repel each other to form the gap. However, the LDA gap increases under pressure, and one needs to include a rigid band shift on top of the LDA band structure to reproduce the negative pressure coefficients of the gap.[19,26] Improved band structure approaches such as screened exchange or *GW* find the correct band-gap structure.[25] The PbX compounds exhibit structural transitions under pressure. At high pressures the CsCl structure is found, but in all three compounds one or several intermediate phases of semiconducting character are found. The structural details of these intermediate phases are still debated (see Ref. 18 for a review). Orthorhombic phases have recently been proposed, of *Cmcm* symmetry for PbS (Ref. 27) and of *Pnma* symmetry for PbTe (Ref. 28). An interesting issue in this context is whether the structural transition is induced by the gap closure or a (semi-)metallic state exists in the rocksalt phase prior to the occurrence of the structural transition. There are experimental indications that the latter may be the case in PbSe and PbTe, while the situation is less clear for PbS.[18]

In the present work the electronic structures of PbX compounds are investigated using the quasiparticle self-consistent *GW* approximation (QS*GW*).[29] This approach leads to a correct ordering of the band-gap states as opposed to the LDA, and also to the negative pressure coefficients. We further find that for PbSe and PbTe the gap closes at pressures below the structural transition pressures. At the point of gap closure the band dispersions become linear (Dirac-type) in the vicinity of the L point. Increasing the pressure beyond this point leads to reopening of the gap, now with the opposite order of the L_6 states. At moderate *p* doping it is predicted that the PbX compounds develop a filamental Fermi surface with strong tendency toward nesting (at Q vectors $\sim[100]2\pi/a$), which reflects the dominating $pp\sigma$ bonding interaction.

This paper is organized as follows. In Sec. II the QS*GW* methodology is briefly outlined and calculational details presented. In Sec. III the QS*GW* band structure results for PbS, PbSe, and PbTe are presented and discussed. Finally, Sec. IV gives the conclusions drawn from the present work.

II. METHODOLOGY

The *GW* approximation[30] is formally the first term in an expansion of the nonlocal and energy-dependent self-energy $\Sigma(\mathbf{r},\mathbf{r}',\omega)$ in the screened Coulomb interaction W. A more physically appealing picture views the *GW* as a dynamically screened Hartree-Fock approximation plus a Coulomb hole contribution.[30] The quasiparticle energies ϵ_α and wave functions $\psi_\alpha(\mathbf{r})$ are solutions to the equation

$$\hat{H}_0\psi_\alpha(\mathbf{r}) + \int \Sigma(\epsilon_\alpha,\mathbf{r},\mathbf{r}')\psi_\alpha(\mathbf{r}')d^3r' = \epsilon_\alpha\psi_\alpha(\mathbf{r}), \qquad (1)$$

where $\hat{H}_0$ is the Hamiltonian of a noninteracting reference system, and the self-energy operator Σ in *GW* is expressed as

$$\Sigma(\omega,\mathbf{r},\mathbf{r}') = \frac{i}{2\pi}\int G_0(\omega+\omega',\mathbf{r},\mathbf{r}')W(\omega',\mathbf{r},\mathbf{r}')d\omega'. \qquad (2)$$

In this equation G_0 is the Green's function of the uncorrelated reference system while W denotes the screened Coulomb interaction. Very often G_0 is constructed from an LDA or LDA+U band structure, in which case the reference system strictly speaking is not uncorrelated, but the potential due to correlation is the exchange-correlation potential, V_{xc}, which is explicitly known and can be subtracted: $\Sigma \rightarrow \Sigma - V_{xc}\delta(\mathbf{r}-\mathbf{r}')$. The bare interaction between two electrons in positions $\mathbf{r}$ and $\mathbf{r}'$ is

$$v(\mathbf{r}-\mathbf{r}') = \frac{e^2}{|\mathbf{r}-\mathbf{r}'|}, \qquad (3)$$

where e denotes the electron charge. This interaction potential is screened by the presence of the other electrons in the solid, which is expressed through the dielectric function $\varepsilon(\omega,\mathbf{r},\mathbf{r}')$, so that the effective interaction is

$$W(\omega,\mathbf{r},\mathbf{r}') = \int \varepsilon^{-1}(\omega,\mathbf{r},\mathbf{r}'')v(\mathbf{r}''-\mathbf{r}')d^3r''. \qquad (4)$$

The dielectric function is calculated in the random-phase approximation as $\varepsilon=1-vP$, where the polarization function P is given as $P=-iG_0\times G_0$.

The above equations thus outline a mapping $\hat{H}_0 \rightarrow \Sigma$. However, from the self-energy operator an "optimum" nonlocal one-electron "exchange-correlation" potential may be constructed,[29,31] defining a mapping $\Sigma \rightarrow \hat{H}_0$. The combined mapping may therefore be iterated to self-consistency, and at self-consistency the reference system, described by $\hat{H}_0$, has a band structure as close as possible[29,31] to the true quasiparticle band structure in Eq. (1).

The *GW* approach neglects several contributions to the full self-energy operator, which can be collected as vertex corrections in the *GW* formalism.[30] Leading vertex corrections have been studied in a few cases,[32–34] but the computing effort is large. A simpler empirical approach[35] of reducing the QS*GW* self-energy by a factor 0.8 [hybrid QS*GW* (hQS*GW*) approximation] has been found to lead to good quantitative agreement with experimental gaps in a wide class of semiconductors.

The electronic structure calculations were performed with the linear muffin-tin orbital (LMTO) method[36] in the full-potential version of Ref. 37. Inside muffin-tin spheres, the orbitals are represented by angular sums of numerical radial functions. The orbitals are matched onto smoothed Hankel functions in the interstitial region. Two sets of orbitals, with *spdfg* and *spd* characters, respectively, with different decay rates in the interstitial region, were used on each atomic site. The tails of the orbitals were expanded inside other muffin-tin spheres with a cutoff of $\ell_{max}=6$. Careful checks were made of convergence in the wave-function basis, the product basis, and other parameters. For the wave-function basis, 1-shot LDA-based $G^{\mathrm{LDA}}W^{\mathrm{LDA}}$ calculations were carried out, adding augmented plane waves (APWs) to the generalized LMTO basis.[38] APWs improve the basis in the interstitial regions. The additional APWs affect the band structure very slightly (e.g., gap at L changes by ~0.01 eV).

The basis set included the Pb 5*d* semicore states, treated as local orbitals,[39] since the bands around the fundamental gap are affected by both Pb 5*d* and 6*d* degrees of freedom. For further variational freedom, additional orbitals of *spd* character were centered on interstitial sites, and high-energy Pb and chalcogen $(n+1)s$ and $(n+1)p$ orbitals were included (n meaning the main valence shell), as shallow local orbitals. Local orbitals affect the basis in the augmentation region. These states play a non-negligible role in obtaining an accurate band structure for the unoccupied states, which were included in the calculation of the polarization function up to a cutoff of 40 eV above the CBM.

All scalar-relativistic effects are included in the *GW* calculations, while spin-orbit coupling is not included during the QS*GW* self-consistency iterations but is added as an extra term in the Hamiltonian for the final computation of the quasiparticle band structure. The spin-orbit coupling is significant, and the extra degrees of freedom in the Pb and anion *p* partial waves provided by the local orbitals are needed to reliably capture this within the $\mathbf{L}\cdot\mathbf{S}$ approximation.[40] Tests within the atomic-spheres approximation[36] revealed that the fundamental gap and other aspects of the band structure of the lead chalcogenides are negligibly affected by whether one uses a fully Dirac-relativistic formulation[41,42] or the approximative $\mathbf{L}\cdot\mathbf{S}$ description of spin-orbit interaction. The self-energy is computed by integration over a $8\times8\times8$ k mesh in the BZ.

III. RESULTS AND DISCUSSION

A. Band structures

The self-consistent quasiparticle band structures of PbS, PbSe, and PbTe calculated at the measured low-temperature lattice constants[43] are presented in Figs. 1–3. The PbSe band structure in Fig. 1 shows the Se *s* band at low energy, around −12 eV relative to the valence-band maximum, and the Pb *s* band a little higher, around −8 eV. The states around the gap are dominated by Pb and Se *p* bands, which are highly hybridized, however, predominantly with Se states below and Pb states above the Fermi level. The average direct band gap is 2–3 eV, caused by avoided crossings, which are clearly seen along Γ-X and Γ-K lines. The minimum gap is formed

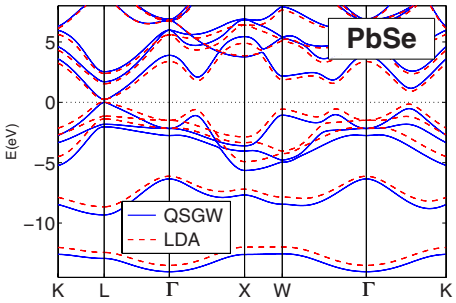

FIG. 1. (Color online) Comparison of QS*GW* (full blue line) and LDA band structures (dashed red line) of PbSe. The zero of energy is placed at the valence-band maximum.

at the L point, where the Se *p* state is pushed up in energy due to antibonding interaction with the Pb *s* state while the Pb *p* state is pushed downward due to hybridization with Se *d* states.[19] Both states have L_6 symmetry but different parity. Putting the Pb atom at the origin, the VBM state is an even L_6^+ state while the CBM state is an odd L_6^- state. Compared to LDA (dashed lines in Fig. 1), the QS*GW* band structure of PbSe displays only minor changes: the average direct band gap is increased by ~0.5 eV, the band width of the Se *p* valence band is increased by ~1 eV, and Pb and Se *s* bands are slightly downshifted in the QS*GW* approximation. These are normal effects of the *GW* approach, and similar effects are observed for PbS and PbTe (the *s* bands are not shown in Figs. 2 and 3). Within the LDA the minimum band gap also occurs at the L point with similar value (E_g =0.26 eV in LDA and E_g=0.21 eV in QS*GW* for PbSe), but behind this lies the fact that the order of valence and conduction states at the L point has been reversed. Away from the L point the corresponding bands repel each other leading in both cases to the opening of a gap, however, in terms of the $E(L_6^-)-E(L_6^+)$ energy difference, the QS*GW* inflicts a correction of 0.47 eV (from −0.26 to +0.21 eV).

The present results for the energy gaps and spin-orbit splittings of the PbX compounds are summarized and compared to experiment in Tables I and II. The QS*GW* gaps are 0.31 eV, 0.21 eV, and 0.29 eV for PbS, PbSe, and PbTe, which compares favorably with the experimental low-temperature values of PbS and PbSe, 0.286 eV and 0.165 eV,

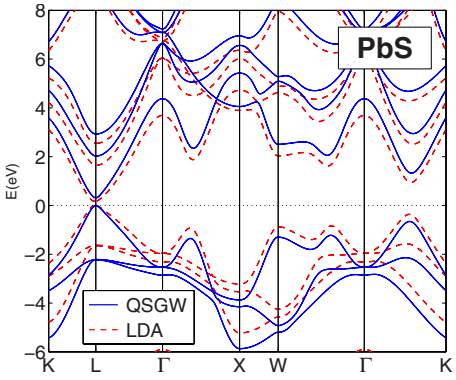

FIG. 2. (Color online) Comparison of QS*GW* (full blue line) and LDA band structures (dashed red line) of PbS. The zero of energy is placed at the valence-band maximum.

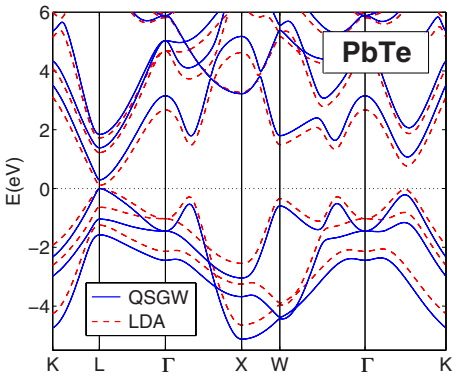

FIG. 3. (Color online) Comparison of QS*GW* (full blue line) and LDA band structures (dashed red line) of PbTe. The zero of energy is placed at the valence-band maximum. The Pb and Te *s* bands are not shown.

respectively, while the experimental value for PbTe is 0.19 eV, i.e., in this case the QS*GW* overestimates the gap slightly more. Overshooting the experimental gap of semiconductors is the expected result for QS*GW*,[31] but the systematics might be different in the IV-VI semiconductors. The LDA gaps agree with previous calculations.[20,22,25] However, for all three compounds the LDA gap is inverted, i.e., with the incorrect $E(L_6^-)<E(L_6^+)$ ordering. Thus, counting the LDA gaps as negative, the correction provided by the QS*GW* approximation amounts to 0.48 eV, 0.47 eV, and 0.40 eV for PbS, PbSe, and PbTe, respectively, i.e., it has similar magnitudes in the three cases. Table I also lists the gaps as calculated with the hybrid QS*GW* approach, which improves the agreement with experiment in many conventional semiconductors,[35] but in the present cases the hybrid approach merely reduces the band gaps by 0.07–0.09 eV with no systematic improvement.

The electron-phonon interaction may influence the value of the energy gap even at zero temperature (due to zero-point

TABLE I. Semiconducting gap of the lead chalcogenides, in eV, as calculated with the QS*GW* approximation, the hybrid (hQS*GW*) approximation and with LDA. Note that the LDA gaps of PbS and PbSe are formed with the wrong order of states at the L point ($L_6^-<L_6^+$), as discussed in the text. Hence they are quoted as negative in this table. The experimental data are low temperature and RT data from Ref. 13. The positive sign of the gap, i.e., $L_6^+<L_6^-$, is experimentally verified through the gap pressure derivative (Ref. 60) and the ^{207}Pb Knight shift (Ref. 11).

	PbS	PbSe	PbTe
QS*GW*, this work	0.31	0.21	0.29
hQS*GW*, this work	0.22	0.14	0.22
LDA, this work	−0.17	−0.26	−0.11
GW[a]	0.35	0.15	0.24
HSE03[a]	0.26	0.13	0.20
Expt.(4.2 K)	0.286	0.165	0.19
Expt. (RT)	0.37–0.40	0.26–0.29	0.29–0.32

[a]The calculations are compared to the *GW* and hybrid-functional calculations of Ref. 25 (HSE03).

TABLE II. Spin-orbit splitting at Γ and X points for the lead chalcogenides, in eV, as calculated with the QS*GW* approximation and with LDA.

	PbS		PbSe		PbTe	
	Γ	X	Γ	X	Γ	X
QS*GW*	0.33	0.28	0.58	0.43	0.99	0.64
LDA	0.36	0.32	0.66	0.48	1.11	0.70
Expt.[a]	0.3	0.2	0.6	0.5	1.15	0.9
Expt.[b]			0.75	0.55	1.10	1.10

[a]The experimental data are from Ref. 61.
[b]The experimental data are from Ref. 23.

motion).[44] This effect was investigated in PbS,[45] in which case a near zero renormalization effect was found due to cancellation of contributions from Pb and S vibrations (contributing −30 and +30 meV to the gap correction, respectively). We do not have access to the required information (electron-phonon interaction strength, isotope effects) to perform a similar analysis for PbSe and PbTe. It seems reasonable, as an estimate, to assume that the major difference will be a rescaling of the chalcogen contribution by the mass factor, $M^{-1/2}$, which would lead to zero-point motion induced gap corrections of −11 meV and −15 meV for PbSe and PbTe, respectively, i.e., hardly of significance in the present context.

The spin-orbit splittings quoted in Table II show good agreement between theory and experiment, except for the splitting at the X point in PbTe, which is 0.64 eV according to the QS*GW* theory but measured to be ~1 eV. It is a consistent trend of the calculations that the spin-orbit splitting is slightly reduced (by about 10%) in QS*GW* compared to LDA, however, both can be said to be in good agreement with the observed numbers.

The photoemission experiments of PbSe and PbTe have been carefully compared to fully relativistic LDA calculations in Ref. 23 with excellent agreement for the band dispersion along the Γ-X direction. While the general topology of the bands is the same in QS*GW* as in LDA, the somewhat wider bands obtained in QS*GW* lead to slightly worsened agreement with experiment. It would be valuable to perform more extensive photoemission studies of the band structures of the lead chalcogenides in order to learn more about the accuracy of the QS*GW* bands.

It is a special feature of the electronic structure of PbX compounds that several secondary maxima of the valence bands occur in the interior of the BZ. Thus, in Figs. 1–3, a secondary valence-band maximum occurs along the Σ line between the Γ and K points while other maxima occur at W and along Γ-X. These maxima reflect a quasicubic filament of high-lying valence states, which originate from the dominating $pp\sigma$-type hybridization of Pb and Te in the highest valence band and lowest conduction band and the avoided crossings of the ensuing bands. This is illustrated in Fig. 4, which shows a surface of constant electron energy $E = E_{\mathrm{VBM}} - 0.30$ eV through the BZ for PbTe. The surface reveals an almost cubic filamental structure with cube corners at the L points. In a rigid band model this energy surface would correspond to the Fermi surface of a hole-doped PbTe sample with about 4% holes/f.u. (as could be realized in a $Tl_xPb_{1-x}Te$ alloy with $x=0.04$). This is somewhat above the region of Tl doping for which superconductivity[9,10] (see, however, Ref. 46) as well as enhanced thermoelectric effect[47] have been reported for $Tl_xPb_{1-x}Te$ samples. It is nevertheless suggestive that these effects originate from the appearance of such a filamental Fermi surface in *p*-doped alloys with accompanying large Fermi surface area and large density of states. On the other hand models of superconductivity[48] in Tl-doped PbTe presume a negative-*U* effect on the Tl *p* states, which does not reconcile with the rigid band model. Figure 5 shows a blowup of the density of states of PbTe around the valence-band maximum. The density of states exhibits a kink at the energy of the secondary valence-band maximum along the Σ line [for PbTe, $E(\Sigma_{max}) = -0.21$ eV]. This kink corresponds to the doping level $x=0.006$. In the theory for the Seebeck effect in metals,[49] the Seebeck coefficient is directly proportional to the slope of the density of states. Hence, it is suggestive that the good thermoelectric performance of PbTe-based materials is at least partly related to the occurrence of these filaments of high-lying hole states. Similar pictures are found for PbS and PbSe, except that in these cases the secondary-band maxima along the Σ line lie

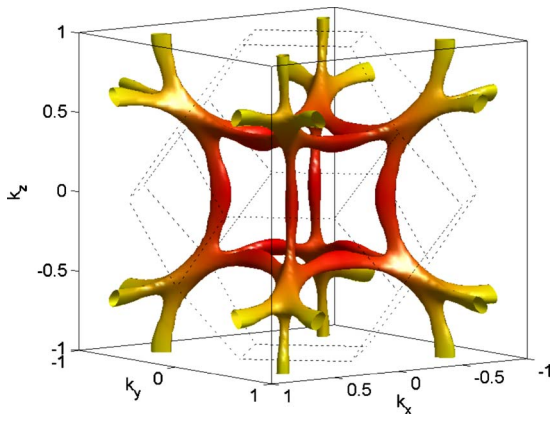

FIG. 4. (Color online) Hole surface in reciprocal space for PbTe in the QS*GW* approximation at $V=V_0$ (Ref. 43). The plot shows the constant energy surface for energy $E=E_{\mathrm{VBM}}-0.30$ eV. The surface is displayed in the double BZ with the fcc BZ sketched by dashed lines. *k* vectors along the axes are in units of $2\pi/a$, where *a* is the lattice constant. The color merely serves visualization purposes.

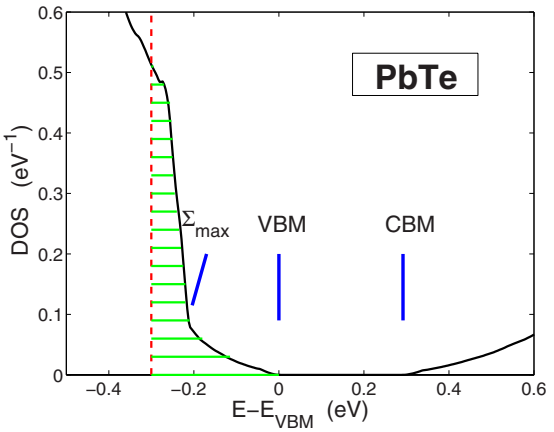

FIG. 5. (Color online) Density of states calculated in the QS*GW* approximation for PbTe in the vicinity of the valence-band maximum. The vertical dashed (red) line corresponds to the energy surface shown in Fig. 4. The hatched area corresponds to about 0.04 holes/f.u. The energies corresponding to the VBM, CBM, and the secondary maximum on the Σ line are marked.

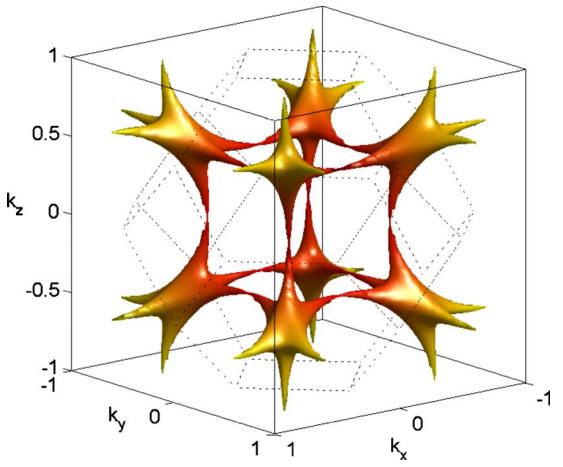

FIG. 6. (Color online) Hole surface in reciprocal space for PbSe in the QS*GW* approximation at $V=V_0$ (Ref. 43). The plot shows the constant energy surface for energy $E=E_{\mathrm{VBM}}-0.54$ eV. The surface is shown in the double BZ with the fcc BZ sketched by dashed lines. k vectors along the axes are in units of $2\pi/a$, where a is the lattice constant. The color merely serves visualization purposes.

deeper [$E(\Sigma_{max})=-0.66$ and -0.52 eV for PbS and PbSe), and, in fact, only constitute saddle points in the energy landscape, as will be discussed further in Sec. III B. In Fig. 6 a similar constant energy plot for PbSe is shown for an energy just below $E(\Sigma_{max})$ (doping level $x=0.05$).

B. Effective masses

The calculated effective masses of the PbX compounds around the L point of the highest valence band and lowest conduction band are listed in Table III. The agreement between the QS*GW* values and experimental data is quite good, in particular taking into account the difficulty of measuring the masses. The calculated values are rather sensitive to the gap, and the band dispersion, in general, is quadratic only in a rather small region around the L point. In their study using the screened exchange interaction, Hummer *et al.* (Ref. 25) found quite accurate gap values and also the masses are in close agreement with experiment. We have included their results for comparison in Tables I and III. One notices a relatively large value of the longitudinal mass in PbTe (i.e., for k vector along the Γ-L direction), which is 9–12 times larger than the transverse mass according to the calculation, 10–14 times larger according to experiment (Ref. 50 even quotes a ratio of 18 ± 4 for holes). For PbS and PbSe the similar factor is ~1.4 and around 2 as given by experiment, and 1.1 and 1.6 as obtained from the theory. The longitudinal mass is always the larger, except for electrons in PbS, where the transverse mass is calculated to be slightly larger than the longitudinal electron mass while experiment has the longitudinal mass 30% larger. The large ratio of longitudinal to transverse mass in PbTe reflects the very elongated electron and hole pockets around the L point, as illustrated in Fig. 7 for holes.

To investigate the importance of the gap size for the derived masses, Table III also lists masses obtained by adjusting the calculated gaps to the experimental low-temperature values. The adjustment procedure simply mixes the QS*GW* self-energy and the LDA exchange-correlation potentials, $\Sigma_{adj}=x\Sigma_{\mathrm{QS}GW}+(1-x)V_{xc}$, i.e., instead of considering a fixed mixing fraction $x=0.8$ as in the hybrid approximation discussed in Sec. II, we use the parameter x to tune to the experimental gap. Values of $x=0.94$, 0.87, and 0.68 provide the desired gaps for PbS, PbSe, and PbTe, respectively. One notices a closer accordance with the experimental transverse masses upon gap adjustment for PbTe and PbSe while the PbSe longitudinal masses are significantly improved and the PbTe longitudinal masses slightly worsened. For PbS, the adjustment has relatively small effect, but in the direction of worsening the agreement with the experimental masses.

The characteristics of the secondary maximum at the Σ point in PbTe has been the subject of several experimental studies in the past. Due to its proximity in energy (even moving closer to the valence-band maximum with temperature) holes are generated in these maxima and their properties may be investigated.[50–53] Table IV lists calculated energies and masses for this point for all three compounds. However, for PbS and PbSe this is not a local maximum in the three-dimensional energy landscape but only a saddle point (hence leading to a large negative mass for one of the principal directions). Since this point is also deeper in energy for PbS and PbSe compared to PbTe it will not be relevant for thermally activated hole carriers, although it might be probed by photoemission spectroscopy.

The effective masses at the Σ point in PbTe for the three principal directions are distinctly different, with one transverse mass being 22 times larger than the longitudinal mass (longitudinal here meaning for motion along the direction of $\mathbf{k}_\Sigma$), and the second transverse mass being an additional factor of 3 smaller. Consequently, the hole pockets around the Σ maximum become very elongated, with a shape like a pea pod, as illustrated in Fig. 8. The direction of the pocket is along the cubic directions of the filamentary structure illustrated in Fig. 4. This picture has also been confirmed by experiment.[50] The corresponding large negative masses for

TABLE III. Effective masses (in units of the free-electron mass) of holes (h) and electrons (e) in PbS, PbSe, and PbTe, at the L point. Values as calculated in the present work with QS*GW* and with the adjusted QS*GW* (aQS*GW*, see text for details) are compared to the masses as calculated with the hybrid-functional approach of Ref. 25 (HSE03), as well as to experimental values from Ref. 11. The last two lines give the calculated volume derivatives of the masses, $\gamma(m)=dm/d\ \ln\ V(V=V_0)$, also in units of the free-electron mass.

		PbS		PbSe		PbTe	
		h(L)	e(L)	h(L)	e(L)	h(L)	e(L)
QS*GW*	$m_{\parallel}$	0.092	0.085	0.080	0.074	0.338	0.247
	$m_{\perp}$	0.073	0.087	0.045	0.049	0.029	0.028
aQS*GW*	$m_{\parallel}$	0.087	0.081	0.066	0.063	0.271	0.209
	$m_{\perp}$	0.071	0.083	0.040	0.042	0.022	0.021
HSE03	$m_{\parallel}$	0.103	0.096	0.075	0.070	0.296	0.223
	$m_{\perp}$	0.071	0.081	0.040	0.041	0.029	0.027
Expt.	$m_{\parallel}$	0.105(15)	0.105(15)	0.068(15)	0.070(15)	0.31(5)	0.24(5)
	$m_{\perp}$	0.075(10)	0.080(10)	0.034(7)	0.040(8)	0.022(3)	0.024(3)
QS*GW*	$\gamma(m_{\parallel})$	1.5	1.3	1.8	1.5	3.2	1.3
	$\gamma(m_{\perp})$	0.6	0.7	0.7	0.7	0.3	0.3

this direction calculated for PbS and PbSe of course imply that the energy dispersion is also very flat in this direction for these two compounds, albeit curving upward, which then also explains the peculiar hole surface illustrated in Fig. 6. There is experimental information available for the secondary maximum of PbTe, which is quoted in Table IV. From the temperature dependence of hole-carrier density the geometric mean $m_c=(m_{\perp z}m_{\parallel}m_{\perp xy})^{1/3}$ may be estimated, although the analysis is sensitive to the modeling of the temperature dependence of the energy of the Σ maximum. The present calculated value of $m_c=0.32$ is in good agreement with the available experimental data. The large anisotropy is confirmed by experiments, which have estimated a value of 10 ± 4 for the ratio of the largest mass to the average of the two smaller masses.[50] The corresponding value calculated in the present work is 36, which can be considered a satisfactory agreement given the uncertainty of the experimental analysis.

C. Pressure effects

The energy gaps of the PbX compounds decrease under pressure. Table V lists the calculated deformation potentials

$$\gamma=\frac{dE_g}{d\ \ln\ V},$$

which are all positive, in agreement with experiment but in contrast to the values calculated within LDA. As discussed, the sign error of the LDA values for γ is due to the inverted gap structure. The calculated QS*GW* values of the deformation potentials compare favorably with experimental values. Several issues hinder the comparison, however. First, the present calculations refer to a static lattice, while experiments usually are done at room temperature and are thus affected by thermal expansion and electron-phonon interaction.[44,45] Second, the deformation potential is the natural quantity to calculate while the natural quantity to measure is the pressure coefficient of the band gap, $\frac{dE_g}{dp}$. The conversion factor is the bulk modulus but there is a considerable spread in experimental values (see Ref. 19). The calculated LDA values of the bulk moduli are $B=65.3$ GPa, 59.6 GPa, and 48.9 GPa, for PbS, PbSe, and PbTe, respectively, which fall within the ranges of experimental values, and they are also similar to those found in previous theoretical works.[19,22] Thermal expansion is equivalent to a negative pressure, so combining the calculated deformation potentials with experimental expansion coefficients of PbX compounds, which are all close to 2.0×10^{-5} K^{-1} at 300 K (linear expansion, from Ref. 16), we arrive at the thermal-expansion coefficients for the energy gap of lead chalcogenides (due to lattice expan-

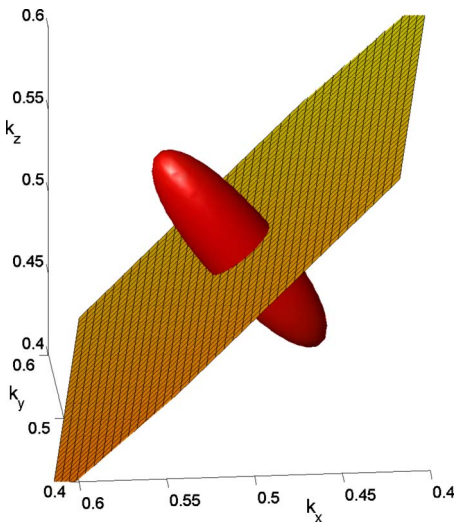

FIG. 7. (Color online) Hole pocket in PbTe in the vicinity of the L point [at coordinates (0.5,0.5,0.5), units of reciprocal vectors are $2\pi/a$, where a is the lattice constant]. The hexagonal BZ facet is indicated. The elongated shape of the hole pocket reflects the large difference in transverse and longitudinal masses. The surface corresponds to the energy $E=E_{\mathrm{VBM}}-0.10$ eV (doping level $x=0.001$).

TABLE IV. Characteristic parameters for the local valence-band maximum along the Σ line in PbS, PbSe, and PbTe. The location of the maximum is given as $\mathbf{k}_\Sigma=(k_\sigma,k_\sigma,0)\ 2\pi/a$. $E(\mathbf{k}_\Sigma)$ is the energy of the maximum relatively to the valence-band maximum, and $m_\parallel$, $m_{\perp xy}$, and $m_{\perp z}$ the effective masses (in units of the free-electron mass) of holes along the three principal axes (1,1,0), (1,−1,0), and (0,0,1), respectively. Finally, m_c is the density-of-states mass, i.e., the geometric mean of the (absolute value of) the masses. Values are calculated in the present work with QS*GW*.

			PbTe	
	PbS, QS*GW*	PbSe, QS*GW*	QS*GW*	Expt.
k_σ	0.416	0.403	0.369	
$E(\mathbf{k}_\Sigma)$ (eV)	−0.66	−0.52	−0.21	−0.14,[a,d] −0.17,[b] −(0.15–0.20) [c]
$m_\parallel$	0.168	0.154	0.171	
$m_{\perp xy}$	0.115	0.089	0.056	
$m_{\perp z}$	−2.51	−8.00	3.54	
m_c	0.36	0.48	0.32	0.11–0.45,[a] 0.38,[c] 0.11,[d] 0.19[e]
$m_{\perp z}/(m_\parallel m_{\perp xy})^{1/2}$	−18	−68	36	10 ± 4 [b]

[a]Reference 52.
[b]Reference 50.
[c]Reference 53.
[d]Reference 51.
[e]Reference 54.

sion alone) of $dE_g/dT=0.32$ meV/K, 0.29 meV/K, and 0.22 meV/K, for PbS, PbSe, and PbTe, respectively. These can be compared to measured temperature coefficients of the gap of $dE_g/dT=0.45$ meV/K for PbS,[45] 0.51 meV/K for PbSe,[12] and 0.45 meV/K for PbTe.[12] It appears that the experimental thermal coefficients of the gap are significantly larger than can be explained solely by thermal expansion, i.e., the electron-phonon interaction also has a significant influence.[12]

Table V also lists the calculated deformation potential for the secondary valence-band maximum at the Σ point, which is positive and of smaller magnitude than the deformation potential of the fundamental gap. With the sign convention $E(\mathbf{k}_\Sigma)<0$, the positive deformation potential implies that the Σ maximum moves away from the valence-band maximum with compression. Comparing the deformation potentials of the fundamental gap and the Σ maximum one notes that the former is a factor 3–4 times larger than the latter. No experimental value of this quantity is available, however, it is well established that for PbTe the secondary minimum moves closer to the VBM as temperature is raised, which is in accord with the calculated sign of the deformation potential. In their analysis of several transport properties, Harris and Ridley (Ref. 54) used a value of $dE(\mathbf{k}_\Sigma)/dT=0.4$ meV/K, implying degeneracy of the two valence-band maxima at about 450 K. They suggest that the separation between the CBM and the Σ maximum is more or less constant with temperature, while rising temperature leads to a relative downshift of the VBM. From our calculated deformation potential and the thermal-expansion coefficient, we arrive at a value of $dE(\mathbf{k}_\Sigma)/dT=0.05$ meV/K, i.e., much lower than Harris and Ridley's value, implying that thermal expansion by itself cannot explain the behavior of the Σ maximum with temperature. Again, it appears that one needs to consider significant phonon-renormalization effects to explain the observed band-edge behaviors.

The calculated volume derivatives of the effective masses are included in Table III. In this case no experimental values have been reported. The effective masses have positive deformation potentials, i.e., under pressure they decrease. This has its origin in the decrease in the gap under pressure. As the two L_6 states come closer and the bands in the vicinity of L repel each other, the dispersion becomes steeper. At the

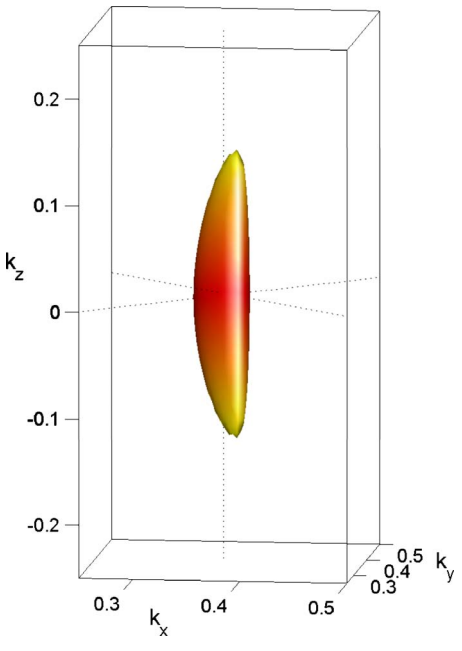

FIG. 8. (Color online) Hole pocket in PbTe in the vicinity of the secondary valence-band maximum along the Σ line. The maximum is located at coordinates $\mathbf{k}_\Sigma=(0.37,0.37,0)$, indicated with the crossing of the dotted lines. Units of reciprocal vectors are $2\pi/a$, where a is the lattice constant. The surface corresponds to the energy $E=E_{\mathrm{VBM}}-0.23$ eV, which is 19 meV below the Σ maximum.

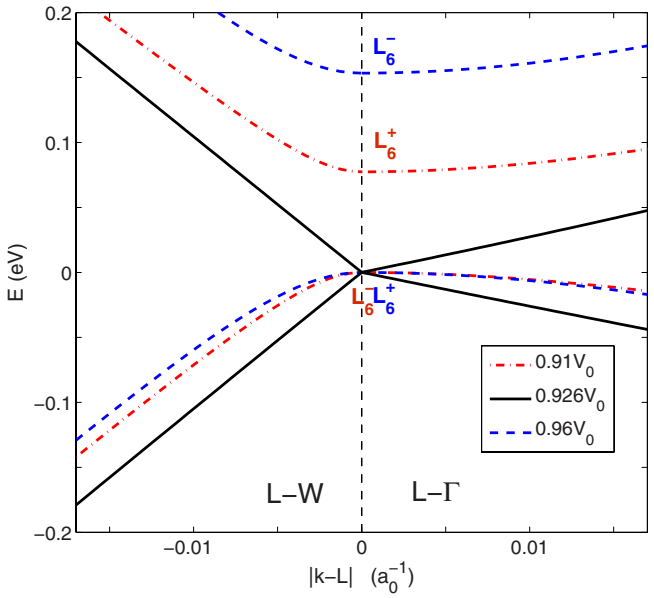

FIG. 9. (Color online) Energy band dispersions around the L point for the highest valence and lowest conduction bands. Three volumes are considered, Ref. 43, corresponding to before gap closure ($V=0.96V_0$, $E_{gap}=0.15$ eV—dashed blue curve), at gap closure ($V=0.926V_0$—full line black curve), and after gap inversion $V=0.91V_0$, $E_{gap}=0.08$ eV—dashed-dotted red curve). The bands are aligned to the VBM. To the left are given bands along the L-W direction (i.e., on the hexagonal face of the BZ), on the right are given bands along the Γ-L direction (i.e., orthogonal to the hexagonal face). The reciprocal vectors are in units of the inverse Bohr radius. The linear dispersions at gap closure, $E=\hbar v\Delta k$, yield velocities $v_\perp=8.5\times10^5$ m/s and $v_\parallel=2.1\times10^5$ m/s for the valence band and $v_\perp=8.4\times10^5$ m/s and $v_\parallel=2.2\times10^5$ m/s for the conduction band.

same time the region around L, where the parabolic approximation for the band dispersion is valid, becomes smaller. From QS*GW* calculations under compression we find the gap closure to happen at the volumes $V=0.94V_0$, $V=0.96V_0$, and $V=0.93V_0$ for PbS, PbSe, and PbTe, respectively, where V_0 denotes the corresponding equilibrium volume.[43] Using the experimental bulk moduli quoted in the caption of Table V, this transforms into the gap closure pressures $p=4.2$ GPa, 2.4 GPa, and 3.4 GPa for PbS, PbSe, and PbTe. These pressures can be compared to the pressures at which the lead chalcogenides undergo structural transitions,[55] which are $p=2.2$ GPa, 4.5 GPa, and 6.0 GPa, respectively. It is thus clear that the pressures at which the gap closure takes place are lower than the structural transition pressures for PbSe and PbTe but higher for PbS. Hence, in principle, the gap closure may be studied in high-pressure experiments on PbSe and PbTe. Indeed there is experimental evidence of a gapless state occurring within the rocksalt phase for PbSe and PbTe,[56] where a maximum in hole mobility as a function of pressure is observed around $p=3$ GPa. On the other hand the situation is unclear for PbS.[18] The observed mobility behavior in PbSe and PbTe is in excellent agreement with the theoretical picture with the gap first shrinking to zero with pressure, then reopening upon further compression (assuming mobility inversely proportional to the gap).[56] In the entire

TABLE V. Deformation potentials (in eV) of the fundamental gap of the lead chalcogenides in eV, as calculated with the QS*GW* approximation, the hybrid (hQS*GW*) approximation and with LDA. The experimental data are converted from measured pressure coefficients, using the bulk moduli $B=70$ GPa (Ref, 27), 60.2 GPa (Ref. 17), and 45.6 GPa (Ref. 17) for PbS, PbSe, and PbTe, respectively. The last row gives the QS*GW* calculated deformation potentials of the secondary valence-band maximum, a positive value implying that this maximum moves closer to the valence band top with volume expansion.

	PbS	PbSe	PbTe
QS*GW*	5.3	4.9	3.6
hQS*GW*	5.0	4.6	3.4
LDA	−3.7	−3.4	−2.3
Expt.	6.3,[a] 3.8–4.9[b]	3.6–5.2,[b] 5.2(5)[c]	3.2–4.1,[b] 3.4(4)[c]
$\gamma[E(\mathbf{k}_\Sigma)]$	1.7	1.6	0.9

[a]Reference 16.
[b]Reference 18.
[c]Reference 17.

pressure range studied here (0–8 GPa), all three lead chalcogenide compounds remain semiconducting, except for semimetallic behavior at the gap closure pressures, i.e., the topology of the bands remain as in Figs. 1–3 and no other secondary valence or conduction edges move close to the L edges.

According to the present QS*GW* calculations, as the gap approaches zero the region around the L point where the band dispersion is quadratic shrinks, and the bands become more and more linear, with perfectly linear (Dirac-type) dispersion when the gap is zero. This is illustrated in Fig. 9 for PbTe, which shows the dispersion in the vicinity of the L point of the highest valence and lowest conduction bands, for three volumes corresponding to before, at, and after band-gap closure. While quite similar before and after the $L_6^-\leftrightarrow L_6^+$ inversion, exactly at gap closure the bands are linear, with different effective velocities along and perpendicular to the Γ-L direction. The linear dispersion might have important consequences such as transformation into topological insulators,[57] as, e.g., could be realized in thin films. The gap closure is well documented in SnPbX alloys (X=Se or Te),[3] since the $E(L_6^-)-E(L_6^+)$ energy difference has the opposite sign in the analogous Sn compounds, however, no observation of linear band dispersion has been reported. We have calculated the QS*GW* band structure of SnSe and SnTe in the rocksalt structure. This is the equilibrium structure for SnTe [above 160 K (Ref. 58)], lattice parameter $a=6.313$ Å. At low temperature, a small rhombohedral distortion of the ideal cubic structure occurs. SnSe has a slightly more distorted structure, while the ideal rocksalt structure may be grown epitaxially on NaCl (Ref. 59) (lattice parameter $a=5.99$ Å). From the calculated QS*GW* gaps for SnTe and SnSe [0.23 and 0.77 eV, both with the correct $E(L_6^-)<E(L_6^+)$ character], the critical concentrations for gap closure may be estimated to be $x_c=0.56$ for $Sn_xPb_{1-x}Te$ and $x_c=0.21$ for $Sn_xPb_{1-x}Se$. For the selenide alloy, this is in excellent agreement with the experimental critical concentrations at low temperature of

x_c=0.15 (Ref. 3), while for the telluride alloy the estimate (x_c=0.56) is significantly larger than the experimental value[3] of x_c=0.35, which reflects the somewhat too large gap of PbTe calculated by the QS*GW* approach in the present work.

IV. CONCLUSION

The band structures of PbS, PbSe, and PbTe semiconducting compounds have been investigated with the quasiparticle self-consistent *GW* approximation. Good accordance with available experimental information is found with this approach, which further facilitates a detailed investigation of effective masses and the pressure effects on these. A quasicubic filamental Fermi surface is found for moderately hole-doped PbX systems, which reflects the *p* bonding of these compounds and the avoided band crossings that lead to the gap formation. At the pressure induced gap closure the highest valence and lowest conduction bands develop linear-dispersion relations as three-dimensional analogs to the graphene Dirac points.

ACKNOWLEDGMENTS

A.S. and N.E.C. acknowledge support from the Danish Center for Scientific Computing Center (DCSC) and the Danish Agency for Science, Technology and Innovation. M.v.S. was supported by NSF under Grant No. QMHP-0802216.

[1] H. Preier, Appl. Phys. **20**, 189 (1979).
[2] I. Melngailis and T. C. Harman, in *Semiconductors and Semimetals*, edited by R. K. Willardson and A. C. Beer (Academic Press, New York, 1970), Vol. 5, p. 111.
[3] D. R. Lovett, *Semimetals and Narrow-Bandgap Semiconductors* (Pion Limited, London, 1979), p. 149.
[4] L. D. Hicks, T. C. Harman, X. Sun, and M. S. Dresselhaus, Phys. Rev. B **53**, R10493 (1996).
[5] T. C. Harman, P. J. Taylor, M. P. Walsh, and B. E. LaForge, Science **297**, 2229 (2002).
[6] M. S. Dresselhaus, G. Chen, M. Y. Tang, R. Yang, H. Lee, D. Wang, Z. Ren, J.-P. Fleurial, and P. Gogna, Adv. Mater. **19**, 1043 (2007).
[7] K. D. Dobson, G. Hodes, and Y. Mastai, Sol. Energy Mater. Sol. Cells **80**, 283 (2003).
[8] N. K. Mudugamuwa, D. M. N. M. Dissanayake, A. A. D. T. Adikaari, and S. R. P. Silva, Sol. Energy Mater. Sol. Cells **93**, 549 (2009).
[9] I. A. Chernik and S. N. Lykov, Sov. Phys. Solid State **23**, 817 (1981).
[10] Y. Matsushita, P. A. Wianecki, A. T. Sommer, T. H. Geballe, and I. R. Fisher, Phys. Rev. B **74**, 134512 (2006).
[11] R. Dalven, in *Solid State Physics*, edited by H. Ehrenreich, F. Seitz, and D. Turnbull (Academic, New York, 1973), Vol. 28, p. 179.
[12] G. Nimtz and B. Schlicht, *Narrow-Gap Semiconductors*, Springer Tracts in Modern Physics Vol. 98 (Springer, Berlin, 1983), p. 1.
[13] W. H. Strehlow and E. L. Cook, J. Phys. Chem. Ref. Data **2**, 163 (1973).
[14] W. Paul and R. V. Jones, Proc. Phys. Soc. London, Sect. B **66**, 194 (1953).
[15] V. Prakash, Harvard University Cambridge Technical Report No. HP 13, 1967 (unpublished).
[16] *Non-Tetrahedrally Bonded Elements and Binary Compounds I*, Landolt-Börnstein New Series Vol. III/41C, edited by O. Madelung, U. Rössler, and M. Schulz (Springer, Heidelberg, 1998).
[17] I. I. Zasavitskii, E. A. de Andrada e Silva, E. Abramof, and P. J. McCann, Phys. Rev. B **70**, 115302 (2004).
[18] S. V. Ovsyannikov, V. V. Shchennikov, A. Y. Manakov, A. Y. Likhacheva, Y. S. Ponosov, V. E. Mogilenskikh, A. P. Vokhmyanin, A. I. Ancharov, and E. P. Skipetrov, Phys. Status Solidi B **246**, 615 (2009).
[19] S.-H. Wei and A. Zunger, Phys. Rev. B **55**, 13605 (1997).
[20] A. Delin, P. Ravindran, O. Eriksson, and J. M. Wills, Int. J. Quantum Chem. **69**, 349 (1998).
[21] A. H. Romero, M. Cardona, R. K. Kremer, R. Lauck, G. Siegle, J. Serrano, and X. C. Gonze, Phys. Rev. B **78**, 224302 (2008).
[22] Y. Zhang, X. Ke, C. Chen, J. Yang, and P. R. C. Kent, Phys. Rev. B **80**, 024304 (2009).
[23] V. Hinkel, H. Haak, C. Mariani, L. Sorba, K. Horn, and N. E. Christensen, Phys. Rev. B **40**, 5549 (1989).
[24] A. Santoni, G. Paolucci, G. Santoro, K. C. Prince, and N. E. Christensen, J. Phys.: Condens. Matter **4**, 6759 (1992).
[25] K. Hummer, A. Grüneis, and G. Kresse, Phys. Rev. B **75**, 195211 (2007).
[26] Z. Nabi, B. Abbar, S. Macabih, A. Khalfi, and N. Amrane, Comput. Mater. Sci. **18**, 127 (2000).
[27] K. Knorr, L. Ehm, M. Hytha, B. Winkler, and W. Depmeier, Eur. Phys. J. B **31**, 297 (2003).
[28] G. Rousse, S. Klotz, A. M. Saitta, J. Rodriguez-Carvajal, M. I. McMahon, B. Couzinet, and M. Mezouar, Phys. Rev. B **71**, 224116 (2005).
[29] T. Kotani, M. van Schilfgaarde, and S. V. Faleev, Phys. Rev. B **76**, 165106 (2007).
[30] L. Hedin and S. Lundqvist, Solid State Phys. **23**, 1 (1970).
[31] M. van Schilfgaarde, T. Kotani, and S. Faleev, Phys. Rev. Lett. **96**, 226402 (2006).
[32] A. J. Morris, M. Stankovski, K. T. Delaney, P. Rinke, P. García-González, and R. W. Godby, Phys. Rev. B **76**, 155106 (2007).
[33] M. Shishkin, M. Marsman, and G. Kresse, Phys. Rev. Lett. **99**, 246403 (2007).
[34] N. E. Christensen, A. Svane, R. Laskowski, B. Palanivel, P. Modak, A. N. Chantis, M. van Schilfgaarde, and T. Kotani, Phys. Rev. B **81**, 045203 (2010).
[35] A. N. Chantis, M. van Schilfgaarde, and T. Kotani, Phys. Rev. Lett. **96**, 086405 (2006).
[36] O. K. Andersen, Phys. Rev. B **12**, 3060 (1975).
[37] M. Methfessel, M. van Schilfgaarde, and R. A. Casali, *Electronic Structure and Physical Properties of Solids*, Lecture Notes in Physics Vol. 535, edited by H. Dreysse (Springer-Verlag, Berlin, 2000), p. 114.

[38] T. Kotani and M. van Schilfgaarde, Phys. Rev. B **81**, 125201 (2010).
[39] D. Singh, Phys. Rev. B **43**, 6388 (1991).
[40] P. Carrier and S.-H. Wei, Phys. Rev. B **70**, 035212 (2004).
[41] N. E. Christensen, J. Phys. F: Met. Phys. **8**, L51 (1978).
[42] N. E. Christensen, Int. J. Quantum Chem. **25**, 233 (1984).
[43] The low-temperature equilibrium lattice constants a=5.909 Å, 6.098 Å, and 6.428 Å were used for PbS, PbSe, and PbTe, respectively (as quoted in Ref. 25). Calculations at compressed volumes are referred to the corresponding volumes, designated V_0 in the text.
[44] M. Cardona and M. L. W. Thewalt, Rev. Mod. Phys. **77**, 1173 (2005).
[45] H. J. Lian, A. Yang, M. L. W. Thewalt, R. Lauck, and M. Cardona, Phys. Rev. B **73**, 233202 (2006).
[46] K. Iakoubovskii, Cent. Eur. J. Phys. **7**, 654 (2009).
[47] J. P. Heremans, V. Jovovic, E. S. Toberer, A. Saramat, K. Kurosaki, A. Charoenphakdee, S. Yamanaka, and G. J. Snyder, Science **321**, 554 (2008).
[48] M. Dzero and J. Schmalian, Phys. Rev. Lett. **94**, 157003 (2005).
[49] J. M. Ziman, *Principles of the Theory of Solids* (Cambridge University Press, Cambridge, 1969).
[50] H. Sitter, K. Lischka, and H. Heinrich, Phys. Rev. B **16**, 680 (1977).
[51] J. R. Dixon and H. R. Riedl, Phys. Rev. **138**, A873 (1965).
[52] R. S. Allgaier and J. B. B. Houston, J. Appl. Phys. **37**, 302 (1966).
[53] N. V. Kolomoets, M. N. Vinogradova, and L. M. Sysoeva, Sov. Phys. Semicond. **1**, 1020 (1968).
[54] J. J. Harris and B. K. Ridley, J. Phys. Chem. Solids **33**, 1455 (1972).
[55] T. Chattopadhyay, H. G. von Schnering, W. A. Grosshans, and W. B. Holzapfel, Physica B & C **139-140**, 356 (1986).
[56] V. V. Shchennikov and S. V. Ovsyannikov, Solid State Commun. **126**, 373 (2003).
[57] L. Fu and C. L. Kane, Phys. Rev. B **76**, 045302 (2007).
[58] V. Fano and I. Ortalli, J. Chem. Phys. **61**, 5017 (1974).
[59] A. N. Mariano and K. L. Chopra, Appl. Phys. Lett. **10**, 282 (1967).
[60] G. Martinez, M. Schlüter, and M. L. Cohen, Phys. Rev. B **11**, 651 (1975).
[61] T. Grandke, L. Ley, and M. Cardona, Phys. Rev. B **18**, 3847 (1978).